

ChemSusChem

Supporting Information

Micropore-Rich Yolk-Shell N-doped Carbon Spheres: An Ideal Electrode Material for High-Energy Capacitive Energy Storage

Xinyuan Li, Zhenhui Liu, Congcong Cai, Qiang Yu, Wenting Jin, Ming Xu, Chang Yu, Shidong Li, Liang Zhou,* and Liqiang Mai*

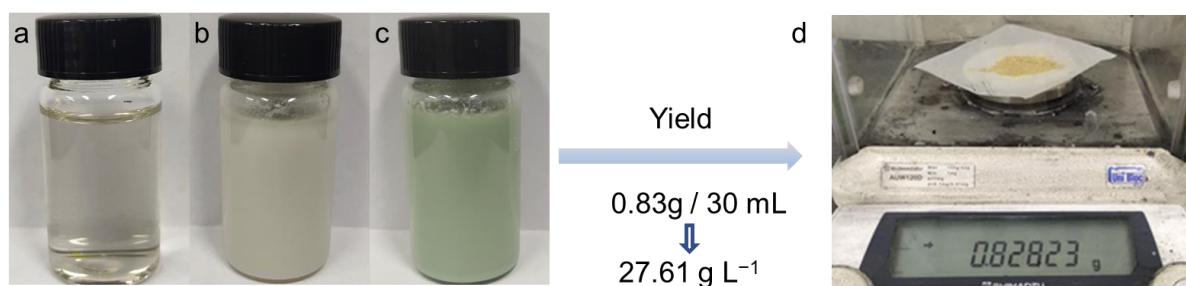


Figure S1. Digital photos of a) 3-aminophenol dissolved in water, b) VTMS hydrolysis completed, and c) resin polycondensation completed. d) Digital photo showing the yield (27.61 g L⁻¹).

Detailed experimental phenomena were recorded. Firstly, 3-aminophenol was dissolved in deionized water to form a colorless and transparent solution. The pH = 7 was neutral, indicating that 3-aminophenol hardly dissociates in water. Subsequently, with the addition of ammonia, VTMS rapidly hydrolyzed at the pH = ~ 10 to form a white turbid solution. Finally, formaldehyde was added for condensation. The color of the solution converted from white to green and the pH was almost unchanged. The yield of one-pot synthesis of VTMS@APF in pure water phase was 27.61 g L⁻¹.

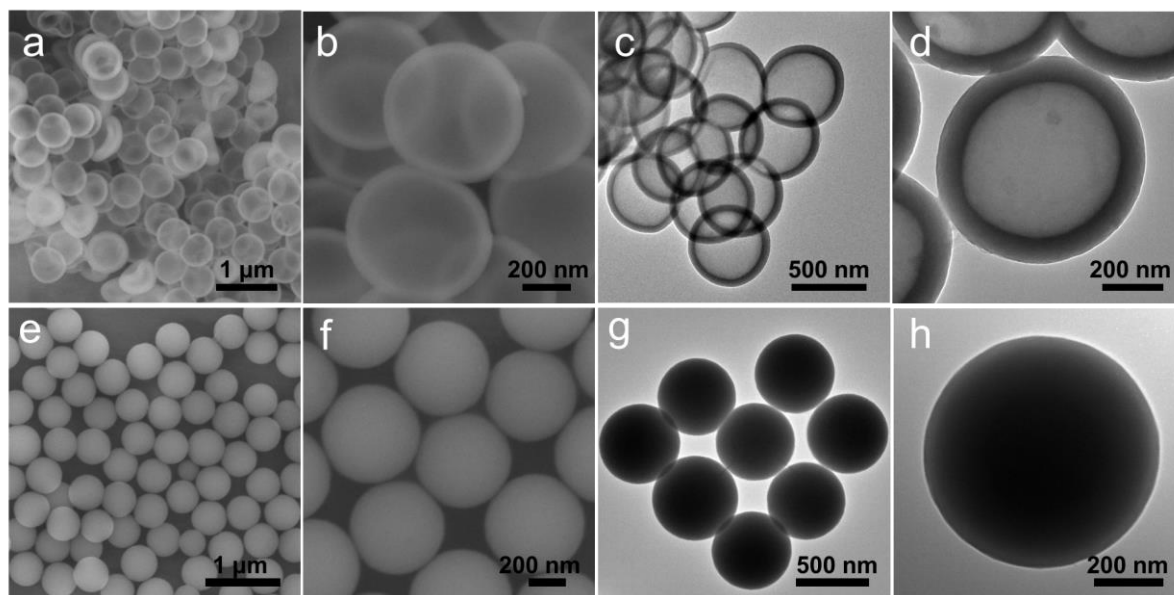


Figure S2. a, b) SEM and c, d) TEM images of H-APF obtained by etching the organosilica@APF with HF; e, f) SEM and g, h) TEM images of SiO₂ obtained by calcinating the organosilica@APF in air.

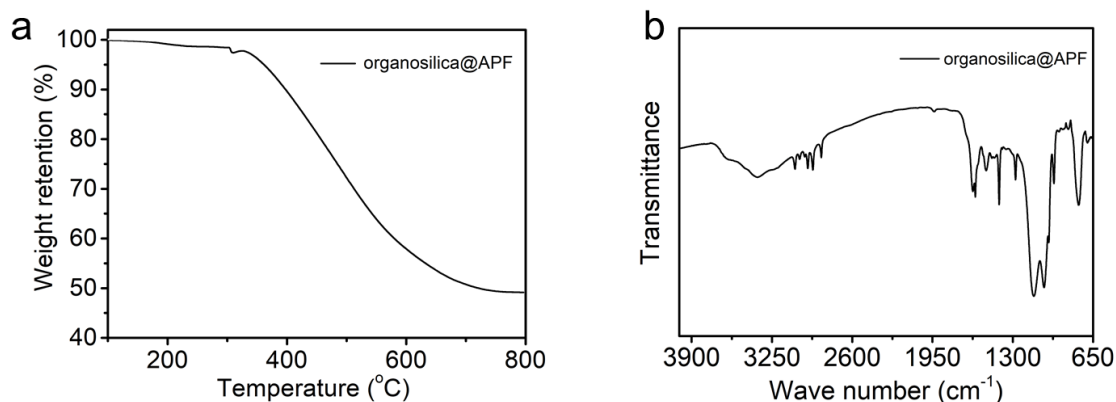


Figure S3. a) TGA curve and b) FTIR spectrum of the organosilica@APF.

The thermal property of organosilica@APF was investigated by TGA. Decomposition of the polymer starts at ~320 °C and the weight loss becomes negligible as the temperature exceeds 750 °C. The as-synthesized organosilica@APF was also characterized using FTIR. The weak absorptions at ~3700 and ~3369 cm⁻¹ correspond to N-H and O-H stretching vibrations, respectively. The absorptions at 3075 and 3026 cm⁻¹ are due to C-H vibrations of -C=C-H. The absorptions at 2975 and 2961 cm⁻¹ are characteristic for the C-H vibrations of -CH₃. The absorptions at 2925 and 2852 cm⁻¹ are due to C-H vibrations of -CH₂-. The absorption at 1626 cm⁻¹ corresponds to C=C vibration of -C=C-. The absorption at 1604 cm⁻¹ are due to C=C vibration of benzene ring. The absorption at 1516 cm⁻¹ correspond to N-H vibration. The absorption at 1412 cm⁻¹ is characteristic for C-N vibration. The absorptions at 1277, 1130, and 1038 cm⁻¹ could be ascribed to C-O stretching vibrations. The absorptions at 1004, 967, and 700 cm⁻¹ correspond to in-plane bending vibration of C-H on benzene ring.

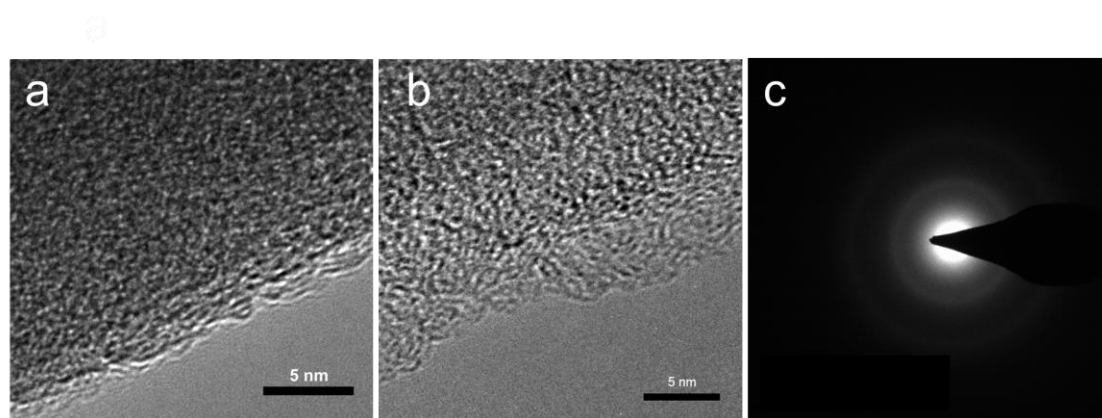


Figure S4. High magnification TEM images: a) YSNCS; b) YSNCS-A. c) SAED pattern of YSNCS-A.

Table S1. Textural properties of YSNCS-A, YP-50F, and NCS-A.

Samples	S_{BET} ($\text{m}^2 \text{g}^{-1}$)	$S_{\text{micro}}^{\text{a}}$ ($\text{m}^2 \text{g}^{-1}$)	V_{t}^{b} ($\text{cm}^3 \text{g}^{-1}$)	$V_{\text{micro}}^{\text{c}}$ ($\text{cm}^3 \text{g}^{-1}$)	V_{n}^{d} (%)	Pore size (nm)
YSNCS-A	2536	2029	1.63	1.41	86.5	2.6
YP-50F	1612	1238	0.80	0.53	66.3	2.0
NCS-A	832	747	0.38	0.29	76.3	1.8

^a Micropore surface area determined by the t-plot. ^b Total pore volume at $P/P_0 \sim 0.99$. ^c Micropore volume. ^d $V_{\text{n}} = V_{\text{micro}}/V_{\text{t}}$. ^e BJH method was applied to analyze the pore size distribution using the desorption branch of the isotherm.

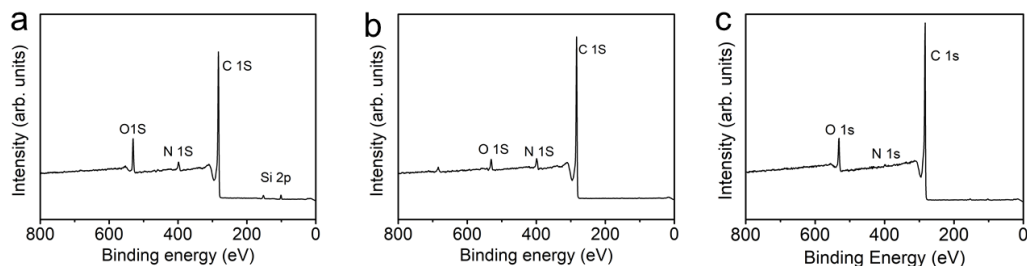


Figure S5. XPS survey spectra: a) $\text{SiO}_x/\text{C}@\text{C}$; b) YSNCS; c) YSNCS-A.

The XPS spectra suggest the co-existence of C, N and O elements in the obtained materials with atomic percentage of 84.5at% C, 4.86 at% N, and 8.37 at% O for $\text{SiO}_x/\text{C}@\text{C}$ (a) , 90.97 at% C, 5.38 at% N and 3.66 at% O for YSNCS (b) , 95.61 at% C, 1.12 at% N, and 3.27 at% O for YSNCS-A (c). The atomic content of Si in $\text{SiO}_x/\text{C}@\text{C}$ is 2.27 at%, indicating that only a small fraction of Si exists in the resin shell (a). The small peak at the binding energy of 685.7 eV in the XPS spectrum of YSNCS (b) can be assigned to the 1 s orbit of F, which is originated from HF etching.

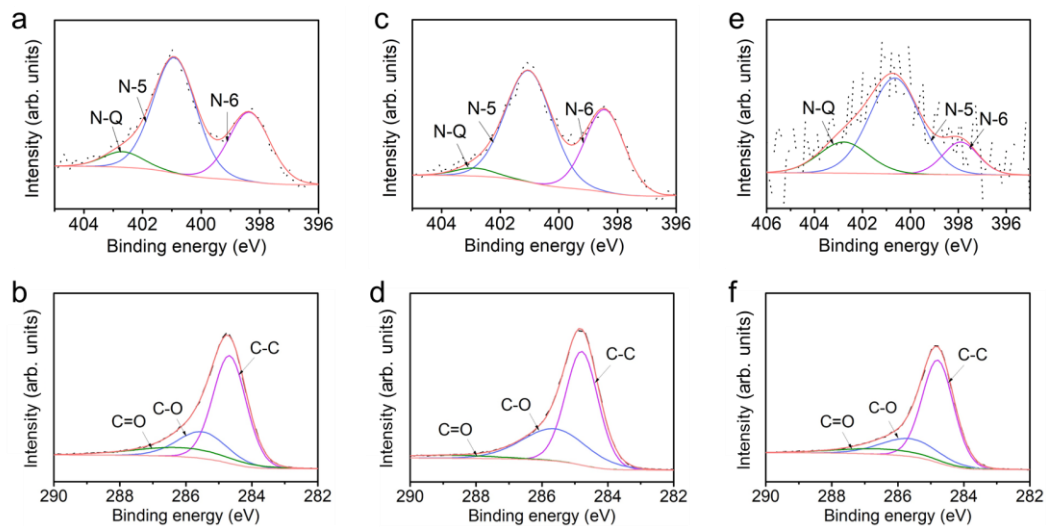


Figure S6. High resolution C1s and N1s spectra of a, b) SiO_x/C@C; c, d) YSNCS; e, f) YSNCS-C. A. The N1s core level spectrum can be fitted into three components, which are attributed to pyridinic nitrogen (N-6) at 398.4 eV, pyrrolic nitrogen (N-5) at 400.9 eV, and graphitic nitrogen (N-Q) at 402.8 eV.

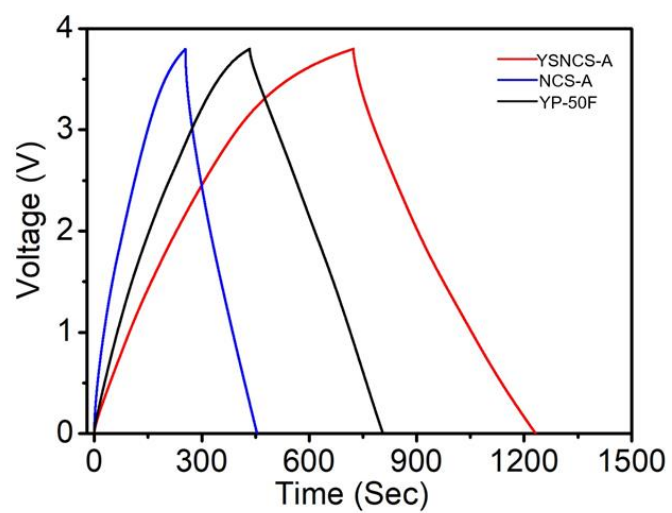


Figure S7. GCD curves of YSNCS-A, NCS-A, and YP-50F at 1 A g^{-1} .

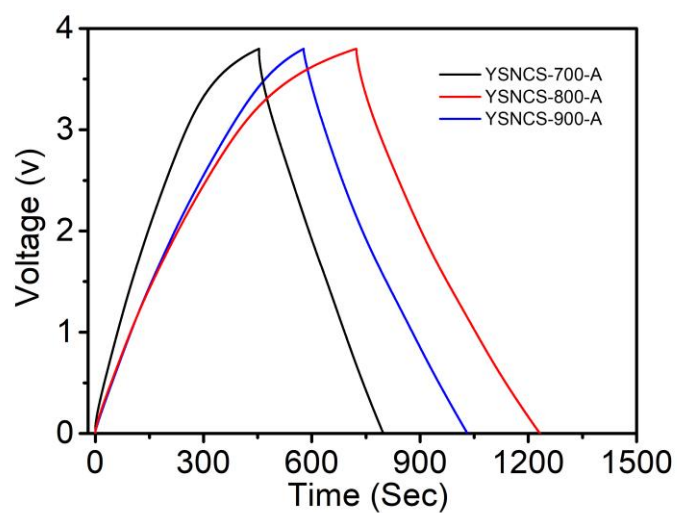


Figure S8. GCD curves of the YSNCS-A samples prepared at carbonization temperatures of 700 °C (YSNCS-700-A), 800 °C (YSNCS-800-A), and 900 °C (YSNCS-900-A) at 1 A g⁻¹.

Table S2. Correlation between the texture structure and electrochemical performance of YSNCS-A and other carbonaceous materials in ILs systems.

Active materials	Peak position of pore size distribution (nm)	SSA ($\text{m}^2 \text{g}^{-1}$)	Electrolyte (mol L^{-1})	Potential window (V)	Current density (A g^{-1})	Mass specific capacity (F g^{-1})	Energy density (Wh kg^{-1})	Power density (W kg^{-1})	Ref.
CCNC1	0.65; 1.25; 15	2561	[EMIM][BF ₄]	4.0	1	205	114	1000	[1]
a-MEGO	0.60; 0.85; 1.50; 4	3100	[BMIM][BF ₄]	3.5	5.7	166	70	10167	[2]
HCP-950	1; 2; 10-70	1831	[Et ₄ N][BF ₄]/ AN (1)	2.7	0.1	127	32	67	[3]
C-0.75-700	1; 3.20	2872	[EMIM][BF ₄]	4.0	0.5	160	92	1000	[4]
ONSC	0.55; 0.80; 1.20; 2.50	2917	[EMIM][BF ₄]	3.5	0.1	194	90	205	[5]
PE-HCP	1; 5; 10	1129	[EMIM][BF ₄]	4	0.5	110	43	387	[6]
EM-CCG	-	-	[EMIM][BF ₄]	3.5	1	167	71	852	[7]
HGF	1.20; 2.30	830	[EMIM][BF ₄]	3.5	20	190	80	6465	[8]
YSNCS-A	0.72; 1.30; 2.75	2536	[EMIM][BF ₄]	3.8	1	269.8	133	943	This work

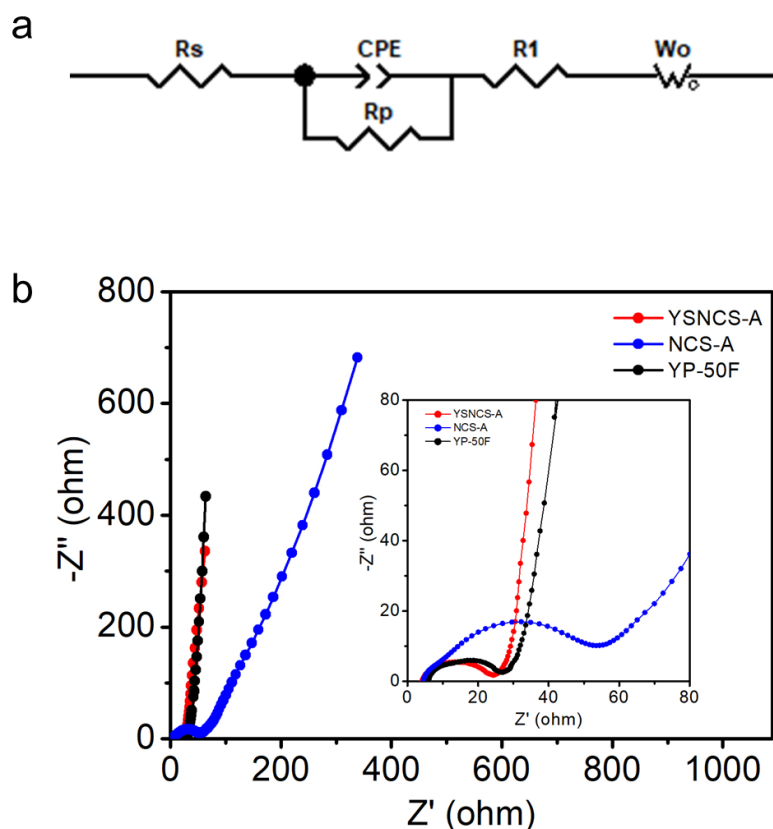


Figure S9. a) The fitted equivalent circuits of the EIS. b) Nyquist plots with fitting curves and the corresponding high frequency ranges (inset) of YSNCS-A, NCS-A, and YP-50F.

EIS analysis was employed to understand the capacitive behavior of the YSNCS-A, NCS-A, and YP-50F. A detailed fitting operation was applied to acquire more accurate evaluation parameters, including the internal resistance (R_s), the constant phase angle element (CPE), the charge transfer resistance (R_p), the ion diffusion resistance (R_1), the Warburg impedance (W_o).

Evidence for sufficient ion diffusion was confirmed by the Nyquist plot. The intercept of the curve at high frequency region represents the device resistance obtained by connecting the intrinsic resistance of the electrolyte, the intrinsic resistance of the separator, and the ohmic resistance of the current in series. The semicircle in the intermediate frequency region is related to the impedance of the electrochemical reaction, and the oblique line in the low frequency region is associated with the diffusion of ions in the electrode.

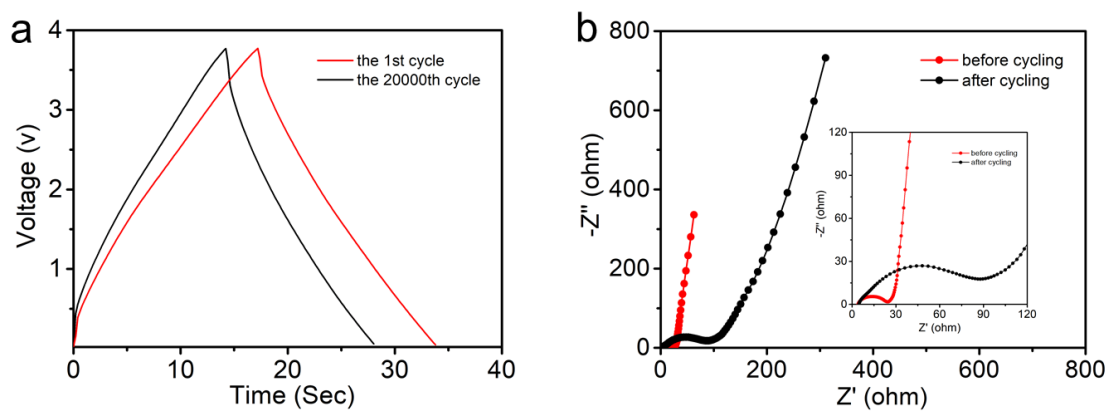


Figure S10. a) GCD curves and b) EIS spectra of YSNCS-A before cycling and after 20000 cycles at 20 A g^{-1} .

Video S1 and Video S2. Digital videos demonstrating the potential of the YSNCS-A based EDLCs to power LEDs and a toy car.

Supplementary References

- [1] Y. Bu, T. Sun, Y. Cai, L. Du, O. Zhuo, L. Yang, Q. Wu, X. Wang, Z. Hu, *Adv. Mater.* **2017**, *29*, 1700470.
- [2] Y. Zhu, S. Murali, M. D. Stoller, K. J. Ganesh, W. Cai, P. J. Ferreira, A. Pirkle, R. M. Wallace, K. A. Cychosz, M. Thommes, D. Su, E. A. Stach, R. S. Ruoff, *Science* **2011**, *332*, 1537.
- [3] H. Wang, S. Yu, B. Xu, *Chem. Commun.* **2016**, *52*, 11512.
- [4] J. Li, N. Wang, J. Tian, W. Qian, W. Chu, *Adv. Funct. Mater.* **2018**, *28*, 1806153.
- [5] Z. Song, H. Duan, L. Li, D. Zhu, T. Cao, Y. Lv, W. Xiong, Z. Wang, M. Liu, L. Gan, *Chem. Eng. J.* **2019**, *372*, 1216.
- [6] Y. Lian, M. Ni, Z. Huang, R. Chen, L. Zhou, W. Utetiwabo, W. Yang, *Chem. Eng. J.* **2019**, *366*, 313.
- [7] X. Yang, C. Cheng, Y. Wang, L. Qiu, D. Li, *Science* **2013**, *341* 535.
- [8] Y. Xu, Z. Lin, X. Zhong, X. Huang, N. O. Weiss, Y. Huang, X. Duan, *Nat. Commun.* **2014**, *5*, 4554.